



ATLAS CONF Note

ATLAS-CONF-2021-045

27th July 2021



A search for an unexpected asymmetry in the production of $e^+\mu^-$ and $e^-\mu^+$ pairs in proton–proton collisions recorded by the ATLAS detector at $\sqrt{s} = 13$ TeV

The ATLAS Collaboration

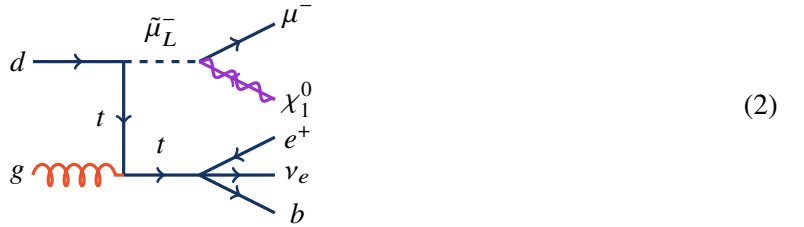
This search, a type not previously performed at ATLAS, uses a comparison of the production cross sections for $e^+\mu^-$ and $e^-\mu^+$ pairs to constrain Beyond Standard Model physics processes. It uses 139 fb^{-1} of proton–proton collision data recorded at $\sqrt{s} = 13$ TeV at the LHC. Targeting sources of new physics which prefer the opposite $e^\pm\mu^\mp$ combination to the Standard Model, the search contains two broad signal regions which are used to provide model-independent constraints on the ratio of cross sections at the 2% level. It also has two special selections targeting supersymmetric models and leptoquark signatures. Observations using one of these are able to exclude singly-produced smuons with masses up to 640 GeV in a model in which the only other light sparticle is a neutralino when the R -parity violating coupling λ'_{231} is close to unity. Observations using the other exclude scalar leptoquarks with masses above 1500 GeV when $g_{1R}^{eu} = g_{1R}^{\mu c} > 0.6$.

1 Introduction

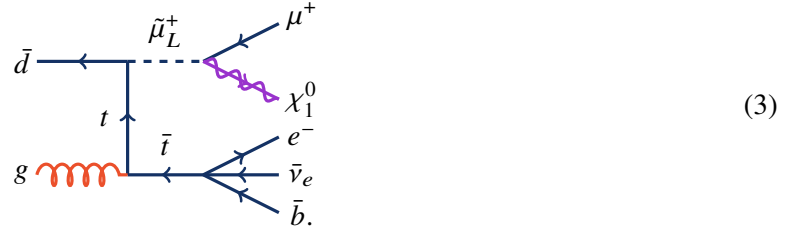
The Standard Model makes a firm prediction for proton–antiproton collisions: it asserts that the cross section for the production of states containing $e^+\mu^-$ should be exactly the same as that for $e^-\mu^+$. For proton–proton colliders the situation is similar but not quite identical. Although the ratio:

$$\rho \equiv \frac{\sigma(pp \rightarrow e^+\mu^- + X)}{\sigma(pp \rightarrow e^-\mu^+ + X)} \quad (1)$$

remains very close to one, spin and phase-space considerations lead to a small bias¹ toward $\rho < 1$, even in the absence of detector effects. It was noted in Ref. [1], however, that a non-zero R -parity-violating λ'_{231} coupling (definition in Ref. [2–4]) linking smuons to top and down quarks could easily drive $\rho > 1$ as the proton’s down quarks would result in:



(and related s -channel processes) occurring more frequently than the charge conjugate process:



The same bias, $\rho > 1$, could instead be driven by the proton’s up quarks if there were a scalar leptoquark with couplings permitting $S_1 \rightarrow ue^-$ and $S_1 \rightarrow c\mu^-$. In that case processes like this:



would be favoured over charge conjugates.

So far as Beyond Standard Model (BSM) *theories* are concerned, there is nothing special about $\rho > 1$. Theories may also be constructed favouring $\rho < 1$. However, it is a curious fact that *experimental* considerations at ATLAS, when taken together with the already-mentioned *physics* bias induced by the pp initial state, make it easier to construct robust searches for $\rho > 1$. The reason for this is that those measurement biases which have a ‘natural’ preference for one charge–flavour combination over the other favour $e^-\mu^+$, and so push charge–flavour universal signals toward smaller values of ρ . More detail on the causes of this preference for one charge–flavour combination over the other may be found

¹ See Appendix A for more on the source of this bias.

in Ref. [1], but the two main issues are: (i) the detector itself is composed of and shielded by material containing matter rather than antimatter, and (ii) the proton–proton initial state is positively charged so that $\sigma(pp \rightarrow W^+ j) > \sigma(pp \rightarrow W^- j)$, yet jets are more likely to be mis-reconstructed as electrons (of either charge) than as muons (of either charge). It should be emphasised that even though this introduction and Appendix A provide physical arguments motivating the Standard Model and experimental biases toward $\rho < 1$, the analysis itself is not reliant on their correctness since it validates their assumptions by checking in data that the event-selections have the expected and desired properties.²

As the first LHC search for charge–flavour violation, this particular analysis looks only for model-independent evidence for $\rho > 1$ so as to exploit the simplifications afforded by the one-sided biases. Future analyses may be designed to make more general tests, albeit at the cost of greater complexity.

The paper concludes by describing two sets of model-dependent exclusions: one in an R -parity-violating supersymmetric model space, and the other in one featuring scalar leptoquarks. It should be emphasised that the fact that the search happens to constrain the models just described is a bonus rather than a goal of the analysis. If there had been no mainstream models able to generate signals with ρ above one we would still have argued that the search was worth doing, even if only to illustrate that data-only self-consistency search techniques can be fun and simple tools with which to look for deviations from the Standard Model.

2 ATLAS Detector

The ATLAS experiment [5] at the LHC is a multipurpose particle detector with a forward–backward symmetric cylindrical geometry and a near 4π coverage in solid angle.³ It consists of an inner tracking detector surrounded by a thin superconducting solenoid providing a 2 T axial magnetic field, electromagnetic and hadron calorimeters, and a muon spectrometer. The inner tracking detector covers the pseudorapidity range $|\eta| < 2.5$. It consists of silicon pixel, silicon microstrip, and transition radiation tracking detectors. Lead/liquid-argon (LAr) sampling calorimeters provide electromagnetic (EM) energy measurements with high granularity. A steel/scintillator-tile hadron calorimeter covers the central pseudorapidity range ($|\eta| < 1.7$). The endcap and forward regions are instrumented with LAr calorimeters for both the EM and hadronic energy measurements up to $|\eta| = 4.9$. The muon spectrometer surrounds the calorimeters and is based on three large superconducting air-core toroidal magnets with eight coils each. The field integral of the toroids ranges between 2.0 and 6.0 T·m across most of the detector. The muon spectrometer includes a system of precision tracking chambers and fast detectors for triggering. A two-level trigger system is used to select events. The first-level trigger is implemented in hardware and uses a subset of the detector information to accept events at a rate below 100 kHz. This is followed by a software-based trigger that reduces the accepted event rate to 1 kHz on average depending on the data-taking conditions.

An extensive software suite [6] is used for real and simulated data reconstruction and analysis, for operation and in the trigger and data acquisition systems of the experiment.

² See later definitions of **CR-RATIO** and **CR-JET**, and the estimates of fake-lepton contributions to Standard Model expectations.

³ ATLAS uses a right-handed coordinate system with its origin at the nominal interaction point (IP) in the centre of the detector and the z -axis along the beam pipe. The x -axis points from the IP to the centre of the LHC ring, and the y -axis points upwards. Cylindrical coordinates (r, ϕ) are used in the transverse plane, ϕ being the azimuthal angle around the z -axis. The pseudorapidity is defined in terms of the polar angle θ as $\eta = -\ln \tan(\theta/2)$. Angular distance is measured in units of $\Delta R \equiv \sqrt{(\Delta\eta)^2 + (\Delta\phi)^2}$.

3 Data and Monte Carlo samples

The proton–proton collisions analysed here were those collected with a centre-of-mass energy of $\sqrt{s} = 13$ TeV and a 25 ns interbunch spacing between 2015 and 2018. They correspond to an integrated luminosity of 139 fb^{-1} with a total uncertainty of 1.7% [7]. In any given data-taking period the un-prescaled two-lepton triggers (specifically ee , $e\mu$ or $\mu\mu$) with the lowest per-lepton p_T thresholds were used [8–10]. These thresholds ranged from 10 GeV to 24 GeV.

R -parity violating (RPV) models were tested using simulated events with $\mu^-\tilde{\chi}_1^0 t$ or $\mu^+\tilde{\chi}_1^0 \bar{t}$ in the final state, where $\tilde{\chi}_1^0$ is the lightest neutralino. This neutralino is considered stable enough on detector scales that it can only be detected through missing transverse momentum, unless it approaches or exceeds the top quark mass, when it can decay through the RPV coupling. These were generated at leading order using **MADGRAPH5_AMC@NLO** [11] version 2.61 together with the RPV MSSM UFO model [12]. Shower evolution and hadronisation was performed by **PYTHIA8** [13] version 8.23. The **NNPDF 2.3 LO PDF** was used with the A14 tune [14]. All RPV couplings except λ'_{231} were set to zero. Supersymmetric particles other than the neutralino and smuon were decoupled by setting their masses to a large value. The **MADGRAPH** hard processes permitted at most one additional light parton in the final state, and they were matched to the **PYTHIA** parton shower using the CKKW-L [15] merging scheme. Use of the merging scale $Q_{\text{MS}} = \frac{1}{4}(m(t) + m(\tilde{\chi}_1^0))$ gives a smooth transitions between Matrix Element and Parton Shower regimes and distributions with little dependence on the exact scale value. MC simulated samples were generated for a two-dimensional grid of points, distributed in a plane of smuon and neutralino masses, all with a coupling of $\lambda'_{231} = 1.0$. Samples for other values of the coupling were obtained by weighting the cross-sections of the first set in proportion to the square of the desired value of λ'_{231} and change in branching ratio for the smuon decay. The branching ratio for the desired smuon to muon decay is 2% (70%) at $\lambda'_{231}=1$ (0.1), whilst the remaining smuons decay via the RPV vertex.

Leptoquark events were generated at leading order using **MADGRAPH5_AMC@NLO** [11] version 2.61 together with the ‘ S_1 ’ model of Ref. [16] which is implemented as a FeynRules [17] package named ‘**LO_LQ_S1**’ available at Ref. [18] and described in Ref. [19]. Shower evolution and hadronisation was performed by **PYTHIA8** [13] version 8.23. The **NNPDF 2.3 LO PDF** was used with the A14 tune [14]. All leptoquark couplings were set to zero apart from two flavours of the g_{1R} coupling of [16] which couples leptoquarks to leptons and quarks in weak singlet states. Specifically g_{1R}^{eu} and g_{1R}^{uc} were assigned a common non-zero value simply denoted “ λ ”. Charm-quark initiated processes are neglected since they provide no charge-flavour asymmetry, and have only $\mathcal{O}(5\%)$ the cross section of the up-quark initiated processes. The hard processes specified no additional light jets in the final state and it was matched to the **PYTHIA** parton shower using the CKKW-L [20] merging scheme. The merging scale Q_{MS} was chosen to be $\frac{1}{4}(m(t) + m(S_1))$, where $m(S_1)$ is the mass of the leptoquark. MC simulated samples were initially generated for a set of leptoquark masses, all with a coupling of $\lambda = 1.0$. Samples for other values of the coupling were obtained by weighting the cross-sections of the first set in proportion to the square of the desired value of λ . A two-dimensional grid of samples for a variety of leptoquark masses and couplings was thereby obtained.

All signal samples were then simulated using **AtFastII** [21], a fast simulation of the ATLAS detector. No uncertainties on the modelling of the signal simulations are considered in the analysis, for either class of models.

Monte Carlo (MC) simulations of SM processes are not used in the final result of this analysis, but were used to guide the signal-region choices, assist in deriving efficiencies and uncertainties for the fake

lepton background estimate, and to make cross-checks (see Appendix B for MC sample details). Instead, measurements of ρ are based entirely on comparisons of $e^+\mu^-$ to $e^-\mu^+$ data, and contributions from jets misidentified as leptons, muon corrections and even expected SM yields (see later) are also estimated primarily from data. The only visible use of Monte Carlo (MC) simulations of SM processes in this note, however, is illustrative: in the lower panel of Fig. 2 they are used to provide a possible breakdown of the expected SM contribution by sub-process.

4 Reconstructed objects

Reconstructed objects (electrons, muons, jets, missing transverse momentum) are the building blocks of any analysis. In this analysis, leptons and jets exist in two forms: ‘**BASELINE**’ and ‘**SIGNAL**’. The former are used to define missing transverse momentum and the overlap removal procedure, otherwise the analysis regions are built exclusively on the latter.

BASELINE electrons are required to have $|\eta| < 2.47$, $p_T > 10$ GeV, and to pass the **Loose** likelihood-based identification working point defined in Ref. [22]. The same p_T and $|\eta|$ demands are placed on **BASELINE** muons, which are also required to pass the **Medium** identification working point as defined in Ref. [23]. The anti- k_t algorithm [24] with a radius parameter of $R = 0.4$ is used to reconstruct jets with a four-momentum recombination scheme, using ‘particle-flow’ objects [25] as inputs. **BASELINE** jets are required to have $p_T > 20$ GeV and $|\eta| < 4.5$. The missing transverse momentum, \vec{p}_T^{miss} , is calculated from the **BASELINE** leptons and jets as described in Ref. [26] using the **Tight** working point and ‘particle-flow track-based soft term’ defined therein.

After the calculation of \vec{p}_T^{miss} (which includes its own overlap removal procedure), an overlap removal procedure is applied to **BASELINE** jets and **BASELINE** leptons to avoid double-counting. Firstly, any electron which shares a track with a muon is rejected. Any jet whose angular distance ΔR from an electron is less than 0.2 is removed, as is any which has fewer than three tracks lying within ΔR of 0.4 of a muon. Finally, electrons and muons within ΔR 0.4 of the remaining jets are then discarded.

The ‘Jet Vertex Tagger’ [27] is applied to jets with $|\eta| < 2.4$, and $p_T < 120$ GeV, and helps to veto jets that are likely to have originated from pile-up. A similar ‘forward Jet Vertex Tagger’ is used to help identify and remove pile-up jets with $|\eta| > 2.5$ [28]. Jets surviving the overlap removal procedure are deemed **SIGNAL** if they pass the Jet and forward Jet Vertex Taggers, the have $|\eta| < 2.8$.

Those leptons which remain are then given a status of **SIGNAL** if they meet the following five criteria: (i) to have $p_T > 25$ GeV, $|\eta| < 2.47$, and (ii) consistency with the primary vertex, through $|d_0(\sigma)| < 3$, and $|z_0 \sin(\theta)| < 0.3$ mm, where d_0 and z_0 are the transverse and longitudinal impact parameters; (iii) electrons must pass the **Tight** likelihood-based identification working point defined in Ref. [22], and have charge-misidentification suppressed through the use of the boosted decision tree based discriminant described in Ref. [22]; (iv) electrons with $p_T < 200$ GeV (or $p_T > 200$ GeV) are required to pass the **FCTight** (resp. **FCHighPtCaloOnly**) isolation working points of Ref. [22] to reduce contamination of electrons from heavy-flavour decays or misidentified light hadrons; and (v) muons with $p_T < 200$ GeV ($p_T > 200$ GeV) are required to pass the **Tight** (resp. **FixedCutHighPtTrackOnly**) isolation working points of Ref. [23] to reduce contamination of muons from semi-leptonic heavy-flavour and hadron decays.

In the rest of the note, leptons and jets are assumed to be only those with **SIGNAL** status, unless stated otherwise.

5 Analysis

The largest source of strictly one-sided charge–flavour bias in the ratio measurement comes from jets in W +jet events being mis-reconstructed as light leptons. In particular: (i) there are more W^+ than W^- produced in LHC proton collisions, and (ii) jets mis-reconstructed as ‘fake’ leptons are more likely to appear to be electrons than muons. If uncorrected these two factors would cause $e_{\text{fake}}^- \mu_{\text{real}}^+$ to be more prevalent than $e_{\text{fake}}^+ \mu_{\text{real}}^-$ and therefore the so-called ‘fake’ background would favour $\rho < 1$. To remove the bias, a data-driven estimate of the number of fake lepton events passing any particular selection is determined and is subtracted from the raw data count before the ratio ρ between $e^+ \mu^-$ and $e^- \mu^+$ counts is calculated. The fake lepton estimate itself is determined using a likelihood-matrix-method approach of the form described in Ref. [29] or ‘Method B’ of Ref. [30]. This method relies on the definition of two lepton definitions of varied stringency. The tighter selection corresponds to the SIGNAL definition used in the rest of the analysis, and the looser ‘LOOSE’ definition relaxes this by removing the isolation requirements, vertex requirements, and loosening the electron identification requirement to the Loose likelihood-based working point defined in Ref. [22]. Real efficiencies are derived in $e^\pm e^\mp$ and $\mu^\pm \mu^\mp$ regions, and fake efficiencies are derived using a muon tag-and-probe method, using $\mu^\pm \mu^\pm$ pairs for the muon efficiency and $e^\pm \mu^\pm$ pairs for the electron efficiency. The efficiencies are calculated separately for each lepton flavour and charge, and are binned in lepton p_T . These efficiencies, together with event counts in regions orthogonal to the signal regions where one lepton is required to pass the LOOSE selection, are used to calculate a prediction for the yield of fake lepton events in the signal regions. The fake lepton estimate accounts for $\mathcal{O}(2\%)$ of the events in the signal regions used for the ratio measurement, and $\mathcal{O}(6\%)$ or $\mathcal{O}(17\%)$ of the events in the signal region used for the RPV supersymmetry and leptoquark interpretations, respectively. As will be seen in Figure 2, the fake estimate is indeed generally higher in $e^- \mu^+$ than $e^+ \mu^-$ events.

The uncertainty on the fake lepton estimate includes two uncertainties: one propagated from uncertainty on the values of the efficiencies, and a “non-closure” uncertainty. The non-closure uncertainty is derived in an $e^\pm \mu^\pm$ region (with the electron failing the SIGNAL selection but passing the LOOSE selection, and the muon passing the SIGNAL selection with an additional requirement of $p_T > 50$ GeV which — like the signal regions — has fake leptons originating predominantly from W +jet events. The difference between the prediction (using Monte Carlo and the data-driven fake estimate) and the data is taken as a non-closure uncertainty, with a magnitude of 21% (13%) for events with $\Sigma(m_T) > 200$ GeV ($\Sigma(m_T) < 200$ GeV).

Only two other source of potential charge–flavour bias motivates application of an explicit correction to data: firstly in certain regions of the detector there are small differences between the reconstruction (and trigger) efficiencies for positively- and negatively-charged muons. These are largely a result of the toroidal magnetic field that the muons move in, relatively increasing the acceptance of one charge of muon in certain regions, usually anti-symmetrically in η . To remove these differences, weights (depending on muon charge, transverse momentum and pseudorapidity, and derived from $Z \rightarrow \mu\mu$ samples following the tag-and-probe approach described in Ref. [31]) are applied to events after data-taking but before any other use in the analysis [32]. These weights correct for the bias by taking the efficiency values back to the charge-averaged values. Approximately two thirds of these weights have values within 1% of unity. In addition to introducing an overall acceptance change of $\sim 0.05\%$, these weights are responsible for event yields acquiring non-integer values. Uncertainties associated with this correction are obtained by propagating the statistical uncertainty on the charge-bias measurement. Secondly, a small correction is applied to data to account for the muon sagitta bias, which is derived according to Ref. [33], and comes with associated uncertainties which are also applied to data. This charge-dependent bias in muon momentum is

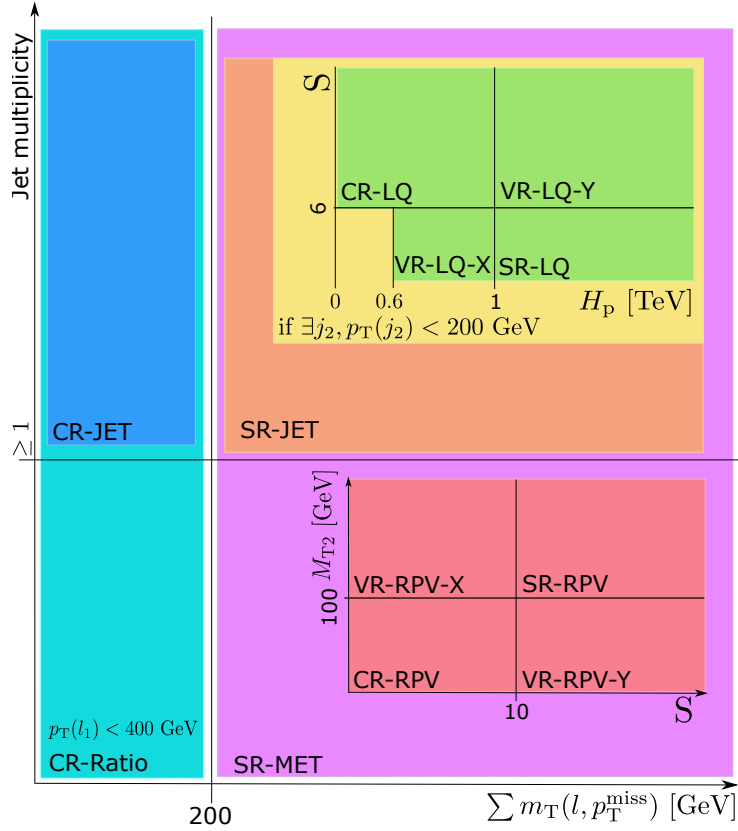


Figure 1: Summary of the regions used in the analysis. l_1 refers to the lepton in each event with the largest p_T . j_2 refers to the jet in each event with the second largest p_T . SR-MET and SR-JET are used for the ρ measurement. CR-RATIO and CR-JET are used to check the SM expectation of $\rho \leq 1$, and CR-RATIO is used to derive the residual-bias uncertainty included in the ratio measurement. CR-RPV is used to derive the SM background expectation used to set limits on RPV supersymmetry models in SR-RPV, after being validated in VR-RPV-X and VR-RPV-Y. CR-LQ is used to derive the SM background expectation used to set limits on scalar leptoquark models in SR-LQ, after being validated in VR-LQ-X and VR-LQ-Y.

caused by mis-alignment of the detector, though is found to be very minor: 68% of muons have a bias of up to 0.2% of muon p_T .

Before unblinding the signal regions, the hypothesis that the proton–proton initial state and experimental effects lead to a bias favouring $\rho \leq 1$ in the SM was confirmed by measuring ρ , binned in M_{T2} , in the region named CR-RATIO as defined in Figure 1. Whilst the ratio is consistent with one within uncertainties, the maximal deviation from one is used to define a 2% ‘residual-bias’ uncertainty encompassing small remaining uncorrected detector biases. The extrapolation of the uncertainty to high $\Sigma(m_T)$ was validated by inspecting its impact on the ρ measurement in CR-RATIO and CR-JET (again defined in Figure 1) when binned in $\Sigma(m_T)$.

The tests of whether ρ is significantly greater than one are made in four signal regions. Two of them, (SR-MET and SR-JET) aim to provide sensitivity to general sources of charge–flavour violation, while the other two (SR-RPV and SR-LQ) are less inclusive version of the partners⁴ which target specific RPV supersymmetry and leptoquark theories mentioned in the introduction. These regions are summarised in Figure 1.

⁴ Every event in SR-RPV is also in SR-MET, and every event in SR-LQ is also in SR-JET.

The **PRELIMINARY** selection common to all signal regions requires the presence of exactly one electron and exactly one muon, of opposite charge. As there are few other constraints on the forms that the signal regions should take, and as the ATLAS experiment has not previously published a charge–flavour asymmetry search, the approach taken in this first search is to prioritise simple selections over complex ones. With this principle in mind:

- when defining **SR-MET**, the only requirement which is added to the **PRELIMINARY** selection is that $\Sigma(m_T) > 200$ GeV where $\Sigma(m_T) \equiv m_T(e, \vec{p}_T^{\text{miss}}) + m_T(\mu, \vec{p}_T^{\text{miss}})$ and m_T is the usual transverse mass:

$$m_T(\ell, \vec{p}_T^{\text{miss}}) \equiv \sqrt{2|\vec{p}_T^\ell| |\vec{p}_T^{\text{miss}}| - 2\vec{p}_T^\ell \cdot \vec{p}_T^{\text{miss}}},$$

- and when defining **SR-JET**, a subset of **SR-MET**, the only additional requirement is that events should contain at least one jet with transverse momentum greater than 20 GeV.

The signal-optimised regions, however, make use of three more flavour-symmetric event variables: \mathcal{S} , M_{T2} and H_P .

- \mathcal{S} is the so-called ‘Object-based \vec{p}_T^{miss} Significance’ defined in equation (15) of Ref. [34]. It is a dimensionless measure of the degree to which the apparent missing transverse momentum in the event is ‘real’ (i.e. attributable to momentum carried away by invisible particles) rather than due to object mis-measurement or pile-up.
- $M_{T2} \equiv \min_{\vec{a}+\vec{b}=\vec{p}_T^{\text{miss}}} \max \left[m_T(e, \vec{a}), m_T(\mu, \vec{b}) \right]$ was proposed in Ref. [35] and is evaluated using the algorithm of Ref. [36].
- $H_P \equiv |\vec{p}_T^e| + |\vec{p}_T^\mu| + |\vec{p}_T^{j_1}|$ is a simple sum of the magnitudes of the transverse momenta of the two leptons and the most energetic jet in the event.

SR-RPV is defined to require $\mathcal{S} > 10$ and $M_{T2} > 100$ GeV. The first requirement anticipates that neutralinos ($\tilde{\chi}_1^0$) of the supersymmetric signals should carry away missing transverse momentum, while the second suppresses SM W^+W^- backgrounds. In all other respects **SR-RPV** is identical to **SR-MET**.

In contrast, the targeted leptoquark-model processes have no invisible particles in the final state, so **SR-LQ** requires $\mathcal{S} < 6$. Furthermore, SM backgrounds in this region are suppressed by requiring events have $H_P > 1$ TeV. In all other respects **SR-LQ** is the same as **SR-JET**.

6 Results

The ratio ρ is measured using a simultaneous profile likelihood fit to observed data ($\vec{N}_{\text{obs},i}^{+-/-}$) in all the bins i of a given variable, taking event yields in each bin and charge–flavour channel ($e^+\mu^-$ or $e^-\mu^+$) to be

independently Poisson distributed, as shown in the expression for the Likelihood:

$$\begin{aligned}
\mathcal{L}(\vec{N}_{\text{obs}}^{+-/-} | \vec{\theta}, \vec{\alpha}, \vec{\rho}) = & \prod_{i \in \text{bins}} \left[\text{Pois}(N_{\text{obs},i}^{-+} | w_i^{-+}(\vec{\theta}) N_{\text{exp},i} + f_i^{-+}(\vec{\alpha}) F_i^{-+}) \right. \\
& \times \text{Pois}(N_{\text{obs},i}^{+-} | \rho_i w_i^{+-}(\vec{\theta}) N_{\text{exp},i} + f_i^{+-}(\vec{\alpha}) F_i^{+-}) \Big] \\
& \times \prod_{k \in \text{fake lepton uncertainties}} \text{Gaus}(0 | \alpha_k, 1) \\
& \times \prod_{j \in \text{data uncertainties}} \text{Gaus}(0 | \theta_j, 1). \tag{5}
\end{aligned}$$

The expected yield for each bin includes the fake lepton background estimate, $F_i^{+-/-}$. Uncertainties (α) associated with the likelihood-matrix-method estimate, and the non-closure uncertainty on the fake lepton background estimate, are considered. These are included as Gaussian nuisance parameters ($\text{Gaus}(0 | \alpha, 1)$), applied to the expected fake lepton background yields through $f_i^{-+/-}(\alpha)$. The expected yield also includes the data with the muon charge and sagitta-bias corrections applied and fake lepton background subtracted $N_{\text{exp},i}$, such that the ratio is measured with these biases removed. The data in the $e^- \mu^+$ channel is used to calculate the expected yield for both channels, with the $e^- \mu^+$ numerator multiplied by the ratio in a given bin ρ_i . Uncertainties (θ_j) associated with the muon corrections are each included as Gaussian nuisance parameters ($\text{Gaus}(0 | \theta_j, 1)$), applied to the expected yields through $w_i^{+-/+}(\vec{\theta})$. The ‘residual-bias’ uncertainty is included in the same manner. P -values are calculated for a one-sided discovery test to exclude the SM hypothesis that $\rho \leq 1$. This uses the profile-likelihood-ratio test statistic, modified to be 0 in the case that the ratio in a bin (parameter of interest) is less than one. This test statistic is converted to a p -value using the asymptotic approximation.

The observed data and fake lepton background estimate in the $e^+ \mu^-$ and $e^- \mu^+$ channels of **SR-MET** and **SR-JET** are shown in Figure 2. The Figure shows the regions binned in the same variables used for the ρ measurement, and in addition shows benchmark RPV-supersymmetry or leptoquark signal yields to demonstrate that these BSM models do favour $e^+ \mu^-$ over $e^- \mu^+$. In the lower panels of the Figure, an estimate of the proportion of SM background processes in each bin is given, showing that $t\bar{t}$ is expected to dominate in most bins apart from the tails, where the fake lepton, diboson, and single top backgrounds become proportionally more important.

The results of the ratio measurement globally in **SR-MET** and **SR-JET** are both $\rho = 0.987^{+0.022}_{-0.021}$, revealing no compelling sign of new physics. These each give a global p -value of 0.5, and the dominant uncertainty contribution is the residual-bias. Binned in M_{T2} and H_{P} , the results of the ratio measurement are shown in Figure 3. In the lower bins of these variables the residual-bias uncertainty dominates, in the final two bins of M_{T2} and three bins of H_{P} the fake lepton and statistical uncertainties dominate. No significant deviation above one is seen in any bin, meaning that the SM hypothesis of $\rho \leq 1$ is not excluded anywhere. The largest deviation of ρ above one has a local significance of merely 1σ . It can also be noted that the largest deviation below one is $\rho = 0.929^{+0.023}_{-0.022}$. This has a local significance of 3.1σ , corresponding to a global significance (associated to the hypothesis that $\rho = 1$) of only 1.6σ .

Having seen consistency with the SM hypothesis in the ratio measurement, limits were placed on the two BSM models. The RPV-supersymmetry model exclusion limits are calculated using a simultaneous profile likelihood fit to data of the $e^+ \mu^-$ and $e^- \mu^+$ channels of both **SR-RPV** and a corresponding control region (**CR-RPV**). As in the ratio measurement, the likelihood here is a product of Poisson probability density functions. The real-lepton SM background estimate for the yield in the $e^- \mu^+$ channel and the

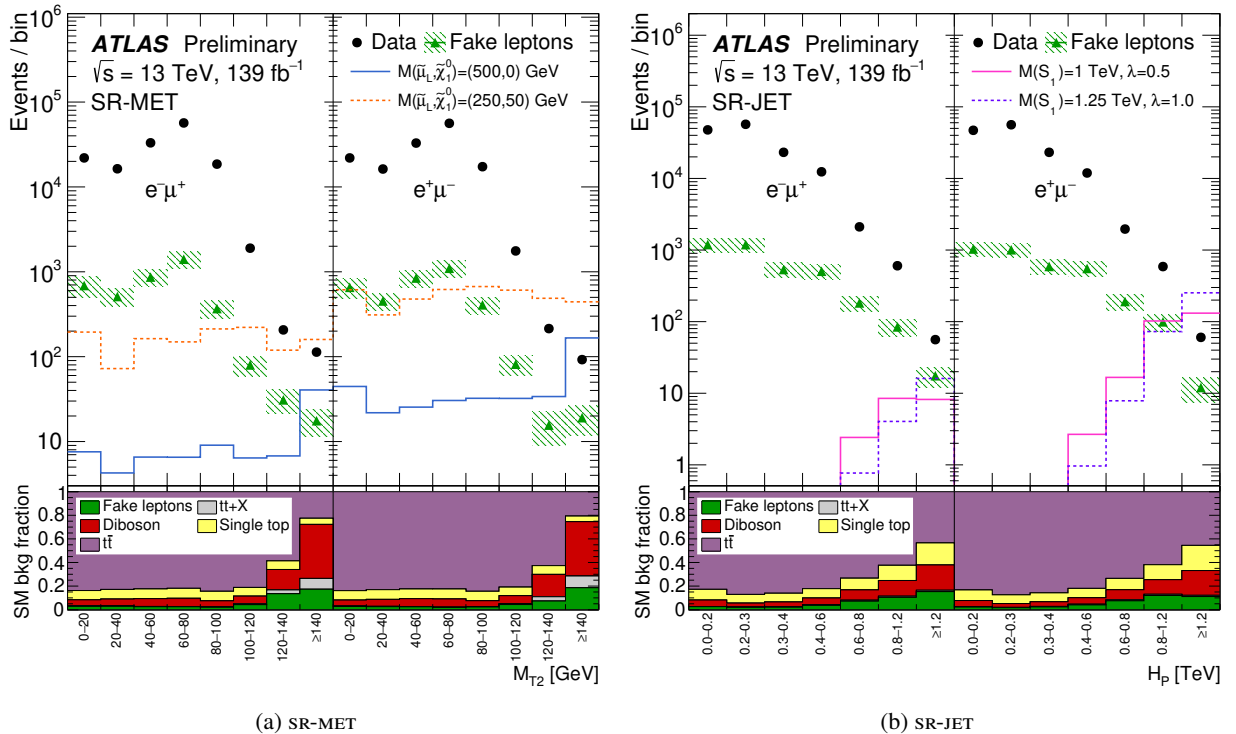


Figure 2: Distributions of data in the $e^+\mu^-$ and $e^-\mu^+$ channels of the general signal regions, binned in M_{T2} for SR-MET, and H_p for SR-JET, to correspond to the ratio measurement binning. The data has the muon charge and sagitta-bias corrections applied and corresponding uncertainties are added in quadrature in the error bar with the statistical uncertainty in data. The fake-lepton background estimate is also shown, along with its uncertainty components added in quadrature, illustrating larger yields in the $e^-\mu^+$ channel as expected. The lower panel shows the fraction that each SM process takes of the total SM background in each bin, estimated using standard MC simulations. $t\bar{t}$ is the dominant background, whilst the importance of the fake background increases in higher bins of each variable. Benchmark RPV-supersymmetry signal models are shown for SR-MET, and benchmark scalar leptoquark models are shown for SR-JET, which all strongly favour the $e^+\mu^-$ final state over $e^-\mu^+$, as expected.

ratio ρ , are constructed using an entirely data-based approach. Analogously to the ratio measurement, the $e^+\mu^-$ denominator expected SM yields are freely-floating nuisance parameters which can constrain themselves to match the data. The $e^-\mu^+$ numerator expected SR yields use these same nuisance parameters, multiplied by ρ . Invariance of the SM ρ (within the uncertainties discussed in the next paragraph) over the (M_{T2}, S) -plane ('RPV-plane') is used, in order to construct control (CR-RPV) and validation regions orthogonal to SR-RPV by inverting both or one of the requirements on these two variables, respectively (Figure 1). Unlike the ratio measurement fit, which has an individual parameter for the ρ value in each bin, there is now one ρ parameter for the entire plane. The SM background estimate is determined during the simultaneous fit to data, such that the value of ρ is determined in the control region, and the expected SM background $e^+\mu^-$ yields in each bin are constrained to match the data. The two validation regions are not included in the fit, but are used to check that the estimate is consistent with data, and thus that ρ is invariant in the plane to the level of precision in the signal region. A second validation of the invariance of the ρ over the plane is performed using a χ^2 test when the plane is binned finely in both directions, leading to a 6% uncertainty applied to ρ that represents variation in ρ over the plane. The overall expected yields in the $e^+\mu^-$ and $e^-\mu^+$ channels also include the fake lepton background estimate. Muon bias corrections and corresponding uncertainties are included.

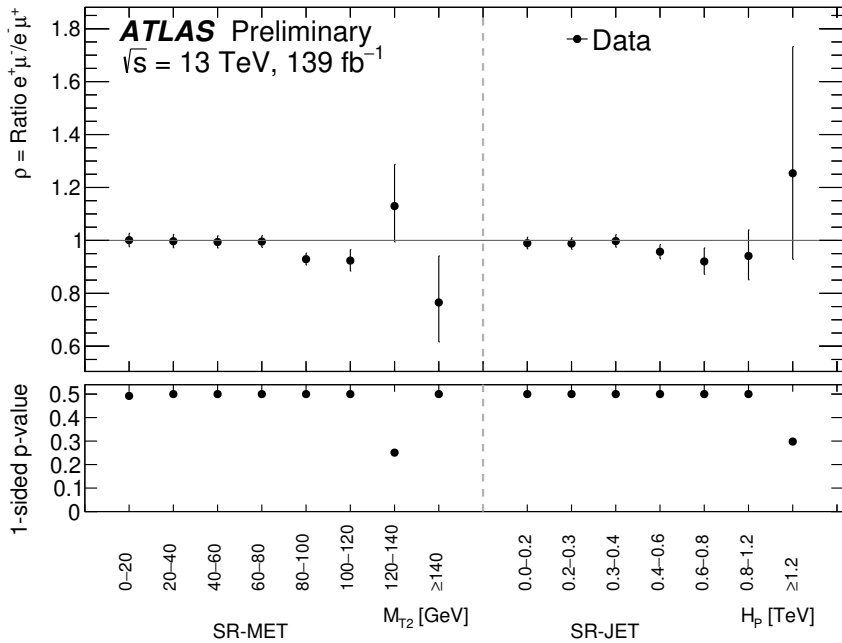


Figure 3: A summary of the ratio ρ measurement in the full Run-2 data for sr-MET binned in M_{T2} , and sr-JET binned in H_p . Muon charge and sagitta bias corrections are applied to data along with corresponding uncertainties, and the likelihood matrix method is used to estimate the charge–flavour-biased fake lepton background such that it can be subtracted from the data. A 2% uncertainty on ρ encompassing remaining observed detector biases is also included. The lower panel shows the p -value for a one-sided discovery test to reject the SM hypothesis that $\rho \leq 1$.

Yields for each RPV-supersymmetry signal point are included, with the muon charge-bias correction and uncertainties applied. Detector uncertainties are applied to the signals. These included uncertainties on lepton reconstruction efficiency, energy scale and resolution, and trigger efficiency difference between MC and data; jet-energy scale and resolution uncertainties [37], uncertainties on the modelling of the \vec{p}_T^{miss} soft term [26], and electron charge identification [38].

As shown in Table 1, no statistically significant deviations are seen between the data and the total SM background prediction. Thus, exclusion limits as 95% CL are computed using the CL_s procedure [39], taking the asymptotic approximation [40].

The observed and expected RPV-supersymmetry limits are shown in Figure 4 for the case where the λ'_{231} coupling is fixed at one, and in Figure 5 where the coupling is varied up to a value of 1.5. The perturbative upper limit for the λ'_{231} coupling is 1.12 at the Z-boson mass [41], and increases with energy scale. For coupling values above 1, the limit at high smuon mass becomes constant as the cross section increase and the branching ratio decrease cancel each other. Neutralino masses near and above that of the top-quark mass are not excluded, as here the neutralino can decay through the RPV coupling and no real \vec{p}_T^{miss} remains in the final state. For the maximal coupling considered, smuon masses are excluded up to 650 GeV.

For the leptoquark model exclusion limits, the same procedure is followed in sr-LQ. Control and validation regions are defined in Figure 1 using the (H_p, S) –plane (‘LQ-plane’), with a 9% uncertainty on the invariance of ρ across it. Again, exclusion limits are set in the absence of any significant disagreement between the data and total SM background prediction, as shown in Table 1. Figure 6 shows the observed and expected limits on the leptoquark models considered.

Table 1: Observed yields, and (post-fit) expected yields for the data-driven SM estimates as well as for the benchmark RPV-supersymmetry signal points in SR-RPV and the leptoquark signal points in SR-LQ. Small weights correcting for muon charge biases affect all rows except that containing the fake lepton estimate. These weights cause non-integer yields. The errors ($\sqrt{(\text{sum of weights})^2}$) are given on data to support the choice to model the yields with a Poisson distribution.

| | SR-RPV | | | SR-LQ | | |
|--|----------------|----------------|--|----------------|----------------|--|
| | $e^+ \mu^-$ | $e^- \mu^+$ | | $e^+ \mu^-$ | $e^- \mu^+$ | |
| $m(\tilde{\chi}_1^0, \tilde{\mu}) = (0, 500) \text{ GeV}, \lambda'_{231} = 1$ | 191 \pm 19 | 46.8 \pm 3.9 | | | | |
| $m(\tilde{\chi}_1^0, \tilde{\mu}) = (50, 250) \text{ GeV}, \lambda'_{231} = 1$ | 1160 \pm 88 | 361 \pm 92 | | | | |
| $m(S_1) = 1000 \text{ GeV}, \lambda = 0.5$ | | | | 157 \pm 26 | 10.6 \pm 2.3 | |
| $m(S_1) = 1250 \text{ GeV}, \lambda = 1.0$ | | | | 244 \pm 38 | 15.9 \pm 3.4 | |
| Data | 489 \pm 22 | 510 \pm 23 | | 60.9 \pm 7.8 | 69.1 \pm 8.3 | |
| Total SM expectation | 503 \pm 48 | 510 \pm 26 | | 61 \pm 13 | 69 \pm 12 | |
| • part due to real leptons | 473 \pm 47 | 479 \pm 24 | | 46 \pm 12 | 47 \pm 11 | |
| • part due to fake leptons | 29.4 \pm 8.2 | 30.3 \pm 8.3 | | 14.1 \pm 4.8 | 22.1 \pm 6.6 | |

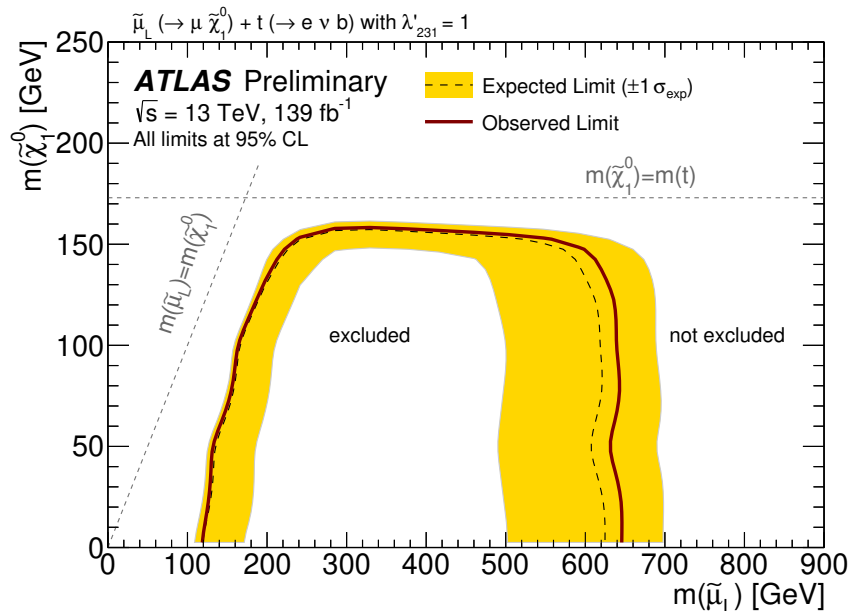


Figure 4: Expected and observed exclusion limits are shown for RPV-supersymmetry models which allow for production of a single smuon (decaying to a muon and neutralino) in association with a top quark (decaying leptonically). The smuon is produced through the λ'_{231} coupling, which is fixed at unity. All limits are computed at 95% confidence level and all uncertainties are included. Also shown are dotted lines to indicate the two kinematic limits for the RPV process considered.

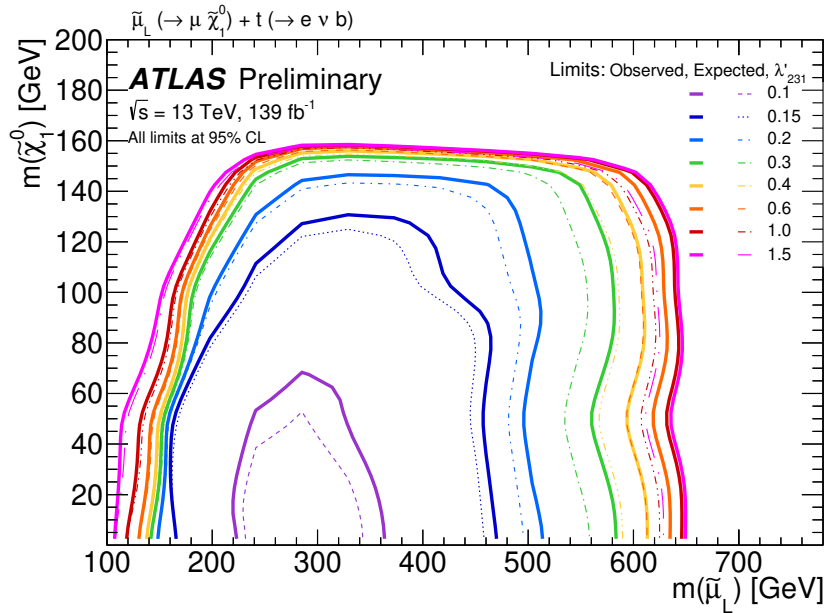


Figure 5: Expected and observed exclusion limits are shown for RPV-supersymmetry models which allow for production of a single smuon (decaying to a muon and neutralino) in association with a top quark (decaying leptonically). The smuon is produced through the λ'_{231} coupling, which takes values up to 1.5. All limits are computed at 95% confidence level and all uncertainties are included.

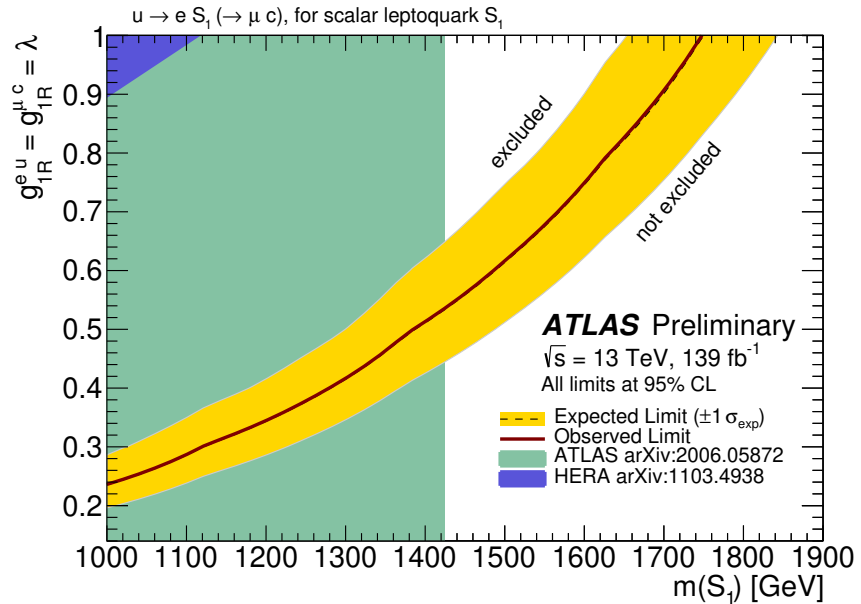


Figure 6: Expected and observed exclusion limits are shown for models featuring single production of a scalar leptoquark followed by decay to a muon and charm quark. All limits are computed at 95% confidence level and all uncertainties are included. The underlaid exclusion is derived from a previous ATLAS leptoquark pair-production search [42], considering only data from μc final states. Since the model in this analysis requires leptoquarks to have two decay modes while that of Ref. [42] assumes only one, the underlaid exclusion uses a branching ratio of 50% into μc to account for the ‘missing’ decays into eu . The interpretation of Ref. [42] also assumes that the narrow width approximation is valid for leptoquarks over the range of coupling values shown.

7 Conclusion

To search for evidence of new physics, this analysis compares the production cross sections for $e^+\mu^-$ and $e^-\mu^+$ by investigating the ratio $\rho = \frac{\sigma(pp \rightarrow e^+\mu^- + X)}{\sigma(pp \rightarrow e^-\mu^+ + X)}$ in a variety of signal regions. According to the Standard Model, this ratio is expected to be marginally less than one in each signal region on account of (i) effects described in Appendix A, and (ii) the “charge-flavour conspiracy” described in Ref. [1]. New physics processes could potentially raise or lower ρ , but even though the largest Standard Model effect known to lower ρ was subtracted, the model-independent tests presented in the first half of this analysis look only for evidence of the ratio being in the ‘unexpected’ region $\rho > 1$. Although this analysis choice inevitably leads to some loss of power⁵, it also leads to simplifications as it removes the need to precisely quantify uncorrected biases whose net effect is to lower ρ . This conservative choice was taken because the present analysis is the first which ATLAS has performed to investigate ρ . More general tests able to look for two-sided departures of ρ from its Standard Model predicted value(s) instead of excesses above 1 are left to future works. No significant model-independent evidence for $\rho > 1$ was seen when analysing 139 fb^{-1} of proton–proton collision data recorded at $\sqrt{s} = 13 \text{ TeV}$ at the ATLAS detector at the LHC.

Further observations were conducted in more exclusive regions optimised for particular beyond Standard Model signals. These regions targeted: (i) R -parity-violating supersymmetric models with non-zero λ'_{231} couplings, with smuons and stable neutralinos, and (ii) scalar leptoquark models with $g_{1R}^{eu} = g_{1R}^{\mu c}$. The secondary measurements were then used to create exclusions in planes in sparticle or leptoquark model spaces. The search was able to exclude singly-produced smuons in certain models in which the only other light sparticle is a neutralino, albeit with those exclusions dependent on the existence of λ'_{231} R -parity-violating couplings. For scalar leptoquark models with $g_{1R}^{eu} = g_{1R}^{\mu c} > 0.5$ the search excluded leptoquark models not targeted by previous analyses.

Appendix A

Pions are the hadrons which are produced most copiously at the LHC, and the charge of the pp initial state leads to a small fractional excess of π^+ over π^- in the final state.⁶ More than 99.98% of these pions decay to muons, and so the resulting excess of secondary μ^+ over μ^- encourages a correspondingly small shift toward $\rho < 1$. The magnitude of this shift is typically suppressed further by the tendency of analyses to target prompt rather than secondary muons. Although there are other charged hadrons whose decays prefer electrons over muons, these are all heavier than the pion and so are less frequently produced. Moreover, when such hadrons are produced the (phase-space induced) factors favouring electrons are all ‘mild’ (i.e. order one) and are therefore unable to overwhelm the (helicity induced) factor of around 8300 by which electrons are suppressed relative to muons in pion decay. The charge of the pp initial state also leads to more production of W^+ than W^- , and as W -boson decays have a preference for muons there is again a tiny bias toward $\rho < 1$. This latter preference is also the result of hadronic effects: it relies on the hadronic and tau-decay modes of the W leading to pion production and a consequent secondary-muon bias which is much larger than (and so overwhelms) the tiny theoretical phase-space enhancement of direct $W^+ \rightarrow e^+\nu$ over $W^+ \rightarrow \mu^+\nu$. In principle a ‘perfect’ isolation requirement (able to separate all secondary-muons from

⁵ This choice makes the analysis insensitive to new physics signals which lower ρ . It is also makes the analysis insensitive to new physics signals which raise ρ by less than the amount which uncorrected biases lower ρ . The latter source of insensitivity is, however, likely to be so small as to be unmeasurable.

⁶ This excess is fractionally small for the simple reason that the number of hadrons in a typical event is very large.

those generated in direct leptonic decays of the W -boson) could be used to suppress the sources favouring $\rho < 1$ over those favouring $\rho > 1$. However, there does not exist, even in principle, an isolation mechanism which is able to suppress secondaries well enough given that $BR(W^+ \rightarrow e^+\nu) = (10.71 \pm 0.16)\%$ only exceeds $BR(W^+ \rightarrow \mu^+\nu) = (10.63 \pm 0.15)\%$ by a small fraction of a percent [43]. The resulting $\rho < 1$ bias is thus small overall, and would change to $\rho > 1$ at a $\bar{p}p$ -collider.

Appendix B

The top pair and single-top backgrounds are modelled using PowHEG [44] v2 interfaced to PYTHIA8 [13] and EvtGEN [45] and the NNPDF 2.3 LO [46] PDF. A di-lepton filter was applied to the $t\bar{t}$ and tW processes.

The diboson backgrounds are modelled using SHERPA [47]. Hard processes with zero or one additional jets in the final state are simulated at NLO, while up to three additional jets are included at LO. Version 2.2.2 is used for the fully leptonic final states ($\ell\ell\ell\ell$, $\ell\ell\ell\nu$, $\ell\ell\nu\nu$ and $\ell\nu\nu\nu$) together with the CT10 PDF [48]. For the semileptonic final states ($\ell\ell qq$ and $\ell\nu qq$) SHERPA version 2.2.1 is used with the NNPDF 3.0 NNLO [46] PDF. The loop-induced processes ($gg\ell\ell\ell\ell$, $gg\ell\ell\nu\nu$, $\ell\ell\ell\ell jj$, $\ell\ell\ell\nu jj$ and same-sign $\ell\ell\nu\nu jj$) are generated using SHERPA version 2.1.1 and the CT10 PDF.

The $Z +$ jets background is modelled using SHERPA 2.2.1 with the NNPDF 3.0 NNLO PDF. Up to two jets are generated at NLO and up to four at LO.

The $t\bar{t} + X$ processes are simulated using `AMC@NLO + PYTHIA8`. The EvtGEN program is used for properties of the bottom and charm hadron decays. The events are normalised to their respective NLO cross sections.

References

- [1] C. G. Lester and B. H. Brunt, *Difference between two species of emu hides a test for lepton flavour violation*, **JHEP** **03** (2017) 149, arXiv: [1612.02697 \[hep-ph\]](https://arxiv.org/abs/1612.02697) (cit. on pp. 2, 3, 14).
- [2] V. Barger, G. F. Giudice and T. Han, *Some new aspects of supersymmetry R -parity violating interactions*, **Phys. Rev. D** **40** (9 1989) 2987, URL: <https://link.aps.org/doi/10.1103/PhysRevD.40.2987> (cit. on p. 2).
- [3] D. Choudhury, *R -parity violation at LEP2: virtual effects*, **Physics Letters B** **376** (1996) 201, ISSN: 0370-2693, URL: <https://www.sciencedirect.com/science/article/pii/0370269396002729> (cit. on p. 2).
- [4] H. K. Dreiner, *An Introduction to Explicit R -Parity Violation*, **Adv. Ser. Direct. High Energy Phys.** **21** (2010) 565, ed. by G. L. Kane, arXiv: [hep-ph/9707435](https://arxiv.org/abs/hep-ph/9707435) (cit. on p. 2).
- [5] ATLAS Collaboration, *The ATLAS Experiment at the CERN Large Hadron Collider*, **JINST** **3** (2008) S08003 (cit. on p. 3).
- [6] ATLAS Collaboration, *The ATLAS Collaboration Software and Firmware*, ATL-SOFT-PUB-2021-001, 2021, URL: <https://cds.cern.ch/record/2767187> (cit. on p. 3).
- [7] ATLAS Collaboration, *ATLAS data quality operations and performance for 2015–2018 data-taking*, **JINST** **15** (2020) P04003, arXiv: [1911.04632 \[physics.ins-det\]](https://arxiv.org/abs/1911.04632) (cit. on p. 4).

- [8] ATLAS Collaboration, *Performance of electron and photon triggers in ATLAS during LHC Run 2*, *Eur. Phys. J. C* **80** (2020) 47, arXiv: [1909.00761 \[hep-ex\]](#) (cit. on p. 4).
- [9] ATLAS Collaboration, *Performance of the ATLAS muon triggers in Run 2*, *JINST* **15** (2020) P09015, arXiv: [2004.13447 \[hep-ex\]](#) (cit. on p. 4).
- [10] A. Collaboration, *The ATLAS Inner Detector Trigger performance in pp collisions at 13 TeV during LHC Run 2*, (2021), arXiv: [2107.02485 \[hep-ex\]](#) (cit. on p. 4).
- [11] J. Alwall et al., *The automated computation of tree-level and next-to-leading order differential cross sections, and their matching to parton shower simulations*, *JHEP* **07** (2014) 079, arXiv: [1405.0301 \[hep-ph\]](#) (cit. on p. 4).
- [12] B. Fuks, *Beyond the Minimal Supersymmetric Standard Model: from theory to phenomenology*, *Int. J. Mod. Phys. A* **27** (2012) 1230007, arXiv: [1202.4769 \[hep-ph\]](#) (cit. on p. 4).
- [13] T. Sjöstrand, S. Mrenna and P. Z. Skands, *A Brief Introduction to PYTHIA 8.1*, *Comput.Phys.Commun.* **178** (2008) 852, arXiv: [0710.3820 \[hep-ph\]](#) (cit. on pp. 4, 15).
- [14] ATLAS Collaboration, *ATLAS Pythia 8 tunes to 7 TeV data*, ATL-PHYS-PUB-2014-021, 2014, URL: <https://cds.cern.ch/record/1966419> (cit. on p. 4).
- [15] L. Lönnblad and S. Prestel, *Merging multi-leg NLO matrix elements with parton showers*, *JHEP* **03** (2013) 166, arXiv: [1211.7278 \[hep-ph\]](#) (cit. on p. 4).
- [16] W. Buchmüller, R. Rückl and D. Wyler, *Leptoquarks in lepton-quark collisions*, *Physics Letters B* **191** (1987) 442, ISSN: 0370-2693, URL: <http://www.sciencedirect.com/science/article/pii/037026938790637X> (cit. on p. 4).
- [17] A. Alloul, N. D. Christensen, C. Degrande, C. Duhr and B. Fuks, *FeynRules 2.0 - A complete toolbox for tree-level phenomenology*, *Comput. Phys. Commun.* **185** (2014) 2250, arXiv: [1310.1921 \[hep-ph\]](#) (cit. on p. 4).
- [18] <https://lqnlo.hepforge.org> (cit. on p. 4).
- [19] I. Doršner and A. Greljo, *Leptoquark toolbox for precision collider studies*, *Journal of High Energy Physics* **2018** (2018) 126, ISSN: 1029-8479, URL: [https://doi.org/10.1007/JHEP05\(2018\)126](https://doi.org/10.1007/JHEP05(2018)126) (cit. on p. 4).
- [20] L. Lönnblad, *Correcting the Colour-Dipole Cascade Model with Fixed Order Matrix Elements*, *JHEP* **05** (2002) 046, arXiv: [hep-ph/0112284](#) (cit. on p. 4).
- [21] ATLAS Collaboration, *The ATLAS Simulation Infrastructure*, *Eur. Phys. J. C* **70** (2010) 823, arXiv: [1005.4568 \[physics.ins-det\]](#) (cit. on p. 4).
- [22] ATLAS Collaboration, *Electron and photon performance measurements with the ATLAS detector using the 2015–2017 LHC proton–proton collision data*, *JINST* **14** (2019) P12006, arXiv: [1908.00005 \[hep-ex\]](#) (cit. on pp. 5, 6).
- [23] ATLAS Collaboration, *Muon reconstruction performance of the ATLAS detector in proton–proton collision data at $\sqrt{s} = 13$ TeV*, *Eur. Phys. J. C* **76** (2016) 292, arXiv: [1603.05598 \[hep-ex\]](#) (cit. on p. 5).
- [24] M. Cacciari, G. P. Salam and G. Soyez, *The Anti- $k(t)$ jet clustering algorithm*, *JHEP* **0804** (2008) 063, arXiv: [0802.1189 \[hep-ph\]](#) (cit. on p. 5).
- [25] ATLAS Collaboration, *Jet reconstruction and performance using particle flow with the ATLAS Detector*, *Eur. Phys. J. C* **77** (2017) 466, arXiv: [1703.10485 \[hep-ex\]](#) (cit. on p. 5).

[26] ATLAS Collaboration, *E_T^{miss} performance in the ATLAS detector using 2015-2016 LHC $p\text{-}p$ collisions*, tech. rep., CERN, 2018, URL: <https://cds.cern.ch/record/2625233> (cit. on pp. 5, 11).

[27] ATLAS Collaboration, *Tagging and suppression of pileup jets with the ATLAS detector*, ATLAS-CONF-2014-018, 2014, URL: <https://cds.cern.ch/record/1700870> (cit. on p. 5).

[28] ATLAS Collaboration, *Identification and rejection of pile-up jets at high pseudorapidity with the ATLAS detector*, *Eur. Phys. J. C* **77** (2017) 580, [Erratum: *Eur. Phys. J. C* 77, 712 (2017)], arXiv: [1705.02211 \[hep-ex\]](https://arxiv.org/abs/1705.02211) (cit. on p. 5).

[29] E. W. Varnes, *A Poisson likelihood approach to fake lepton estimation with the matrix method*, (2016), arXiv: [1606.06817 \[hep-ex\]](https://arxiv.org/abs/1606.06817) (cit. on p. 6).

[30] T. P. S. Gillam and C. G. Lester, *Improving estimates of the number of ‘fake’ leptons and other mis-reconstructed objects in hadron collider events: BoB’s your UNCLE*, *JHEP* **11** (2014) 031, arXiv: [1407.5624 \[hep-ph\]](https://arxiv.org/abs/1407.5624) (cit. on p. 6).

[31] ATLAS Collaboration, *Muon reconstruction and identification efficiency in ATLAS using the full Run 2 $p\text{-}p$ collision data set at $\sqrt{s} = 13$ TeV*, (2020), arXiv: [2012.00578 \[hep-ex\]](https://arxiv.org/abs/2012.00578) (cit. on p. 6).

[32] H. Pacey, *Holly Pacey and the Half-Spin Particles: Searching for new physics with leptons at the ATLAS experiment*, PhD thesis: University of Cambridge, 2020, URL: <https://doi.org/10.17863/CAM.62954> (cit. on p. 6).

[33] ATLAS Collaboration, *Alignment of the ATLAS Inner Detector in Run-2*, (2020), arXiv: [2007.07624 \[hep-ex\]](https://arxiv.org/abs/2007.07624) (cit. on p. 6).

[34] ATLAS Collaboration, *Object-based missing transverse momentum significance in the ATLAS detector*, tech. rep., CERN, 2018, URL: <https://cds.cern.ch/record/2630948> (cit. on p. 8).

[35] C. G. Lester and D. J. Summers, *Measuring masses of semi-invisibly decaying particle pairs produced at hadron colliders*, *Phys. Lett. B* **463** (1999) 99, arXiv: [hep-ph/9906349 \[hep-ph\]](https://arxiv.org/abs/hep-ph/9906349) (cit. on p. 8).

[36] C. G. Lester and B. Nachman, *Bisection-based asymmetric M_{T2} computation: a higher precision calculator than existing symmetric methods*, *JHEP* **03** (2015) 100, arXiv: [1411.4312 \[hep-ph\]](https://arxiv.org/abs/1411.4312) (cit. on p. 8).

[37] ATLAS Collaboration, *Jet energy scale and resolution measured in proton-proton collisions at $\sqrt{s} = 13$ TeV with the ATLAS detector*, (2020), arXiv: [2007.02645 \[hep-ex\]](https://arxiv.org/abs/2007.02645) (cit. on p. 11).

[38] ATLAS Collaboration, *Electron and photon performance measurements with the ATLAS detector using the 2015–2017 LHC proton-proton collision data*, *JINST* **14** (2019) P12006, arXiv: [1908.00005 \[hep-ex\]](https://arxiv.org/abs/1908.00005) (cit. on p. 11).

[39] A. L. Read, *Presentation of search results: the CL_S technique*, *J. Phys. G* **28** (2002) 2693 (cit. on p. 11).

[40] G. Cowan, K. Cranmer, E. Gross and O. Vitells, *Asymptotic formulae for likelihood-based tests of new physics*, *Eur. Phys. J. C* **71** (2011) 1554, arXiv: [1007.1727 \[physics.data-an\]](https://arxiv.org/abs/1007.1727) (cit. on p. 11).

[41] B. C. Allanach, A. Dedes and H. K. Dreiner, *Bounds on R -parity violating couplings at the weak scale and at the GUT scale*, *Phys. Rev. D* **60** (1999) 075014, arXiv: [hep-ph/9906209](https://arxiv.org/abs/hep-ph/9906209) (cit. on p. 11).

- [42] ATLAS Collaboration, *Search for pairs of scalar leptoquarks decaying into quarks and electrons or muons in $\sqrt{s} = 13$ TeV pp collisions with the ATLAS detector*, *JHEP* **10** (2020) 112, arXiv: [2006.05872 \[hep-ex\]](https://arxiv.org/abs/2006.05872) (cit. on p. 13).
- [43] P. Zyla et al., *Review of Particle Physics*, *PTEP* **2020** (2020) 083C01 (cit. on p. 15).
- [44] S. Alioli, P. Nason, C. Oleari and E. Re, *A general framework for implementing NLO calculations in shower Monte Carlo programs: the POWHEG BOX*, *J. High Energy Phys.* **1006** (2010) 043, arXiv: [1002.2581 \[hep-ph\]](https://arxiv.org/abs/1002.2581) (cit. on p. 15).
- [45] D. J. Lange, *The EvtGen particle decay simulation package*, *Nucl. Instrum. Meth.* **A462** (2001) 152 (cit. on p. 15).
- [46] R. D. Ball et al., *Parton distributions with LHC data*, *Nucl. Phys. B* **867** (2013) 244, arXiv: [1207.1303 \[hep-ph\]](https://arxiv.org/abs/1207.1303) (cit. on p. 15).
- [47] T. Gleisberg, S. Höche, F. Krauss, M. Schönherr, S. Schumann et al., *Event generation with SHERPA 1.1*, *JHEP* **02** (2009) 007, arXiv: [0811.4622 \[hep-ph\]](https://arxiv.org/abs/0811.4622) (cit. on p. 15).
- [48] H.-L. Lai et al., *New parton distributions for collider physics*, *Phys. Rev. D* **82** (2010) 074024, arXiv: [1007.2241 \[hep-ph\]](https://arxiv.org/abs/1007.2241) (cit. on p. 15).